ACS OMEGA

Open Access

http://pubs.acs.org/journal/acsodf

Article

Unraveling the Molecular Landscape of SCN1A Gene Knockout in Cerebral Organoids: A Multiomics Approach Utilizing Proteomics, Lipidomics, and Transcriptomics

Byumseok Koh, Young Eun Kim, Sung Bum Park, Seong Soon Kim, Jangjae Lee, Jeong Hyeon Jo, KyungJin Lee, Dong Hyuck Bae, Tae-Young Kim, Sung-Hee Cho,* Myung Ae Bae,*, Dukjin Kang,*, and Ki Young Kim*,

Cite This: *ACS Omega* 2024, 9, 39804−39816

Read Online

ACCESS | Metrics & More | Article Recommendations | Supporting Information

ABSTRACT: This study investigates the impact of sodium channel protein type 1 subunit alpha (SCN1A) gene knockout (SCN1A KO) on brain development and function using cerebral organoids coupled with a multiomics approach. From comprehensive omics analyses, we found that SCN1A KO organoids exhibit decreased growth, dysregulated neurotransmitter levels, and altered lipidomic, proteomic, and transcriptomic profiles compared to controls under matrix-free differentiation conditions. Neurochemical analysis reveals reduced levels of key neurotransmitters, and lipidomic analysis highlights changes in ether phospholipids and sphingomyelin. Furthermore, quantitative profiling of the SCN1A KO organoid proteome shows perturbations in cholesterol metabolism and sodium ion transportation, potentially affecting synaptic transmission. These findings suggest dysregulation of cholesterol metabolism and sodium ion transport, with implications for synaptic transmission. Overall, these insights shed light on the molecular mechanisms underlying SCN1A-associated disorders, such as Dravet syndrome, and offer potential avenues for therapeutic intervention.

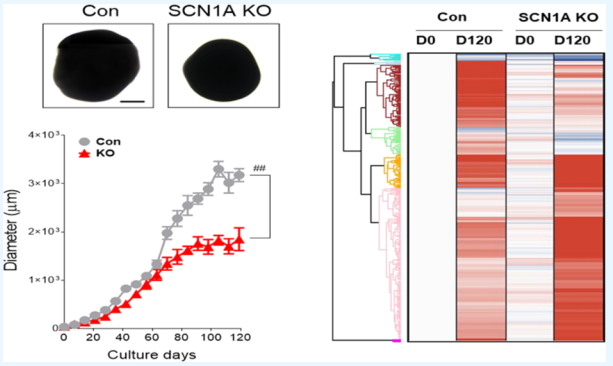

INTRODUCTION

The sodium channel protein type 1 subunit alpha (SCN1A) gene encodes the alpha subunit of the voltage-gated sodium channel Nav1.1, predominantly expressed in neurons within the central nervous system.[1] Mutations in SCN1A are associated with various conditions, including idiopathic epilepsy and genetic epilepsy with febrile seizures, and are particularly relevant to Dravet Syndrome.[2,3] Mouse models with SCN1A knockout exhibit significant disruptions in GABAergic sodium currents,[4] leading to decreased neural inhibition and heightened seizurogenic activity.[5]

Cerebral organoids represent a groundbreaking advancement in neurobiology, offering a three-dimensional *in vitro* model that faithfully recapitulates the structural and functional complexities of the human brain.[6,7] Derived from stem cells, these self-organizing neural structures mimic aspects of embryonic brain development, facilitating the exploration of neuronal migration, synaptic connectivity, and regional differentiation.[8] Additionally, cerebral organoids serve as valuable tools for disease modeling, particularly in the realm of neurodevelopmental and neurodegenerative disorders.[9] A key strength of cerebral organoids is their capability to mimic human-specific aspects of brain development and pathology, providing insights into the interplay between genetic predispositions and environmental influences in neurological disorders.[10,11] Notably, they have been instrumental in recapitulating features of various epileptic conditions, enabling the study of disease progression and the evaluation of potential therapeutic strategies.[12−14]

Moreover, cerebral organoids play a pivotal role in drug discovery and personalized medicine initiatives, offering a platform for testing therapeutic compounds in a human-relevant context.[15] As our understanding of cerebral organoids advances, their significance in elucidating the complexities of brain development and disease pathogenesis is poised to expand, promising transformative impacts on both basic neuroscience research and clinical applications.

While neurotransmitters have long been recognized for their crucial role in neural communication and physiological

Received: May 29, 2024
Revised: August 29, 2024
Accepted: September 5, 2024
Published: September 13, 2024

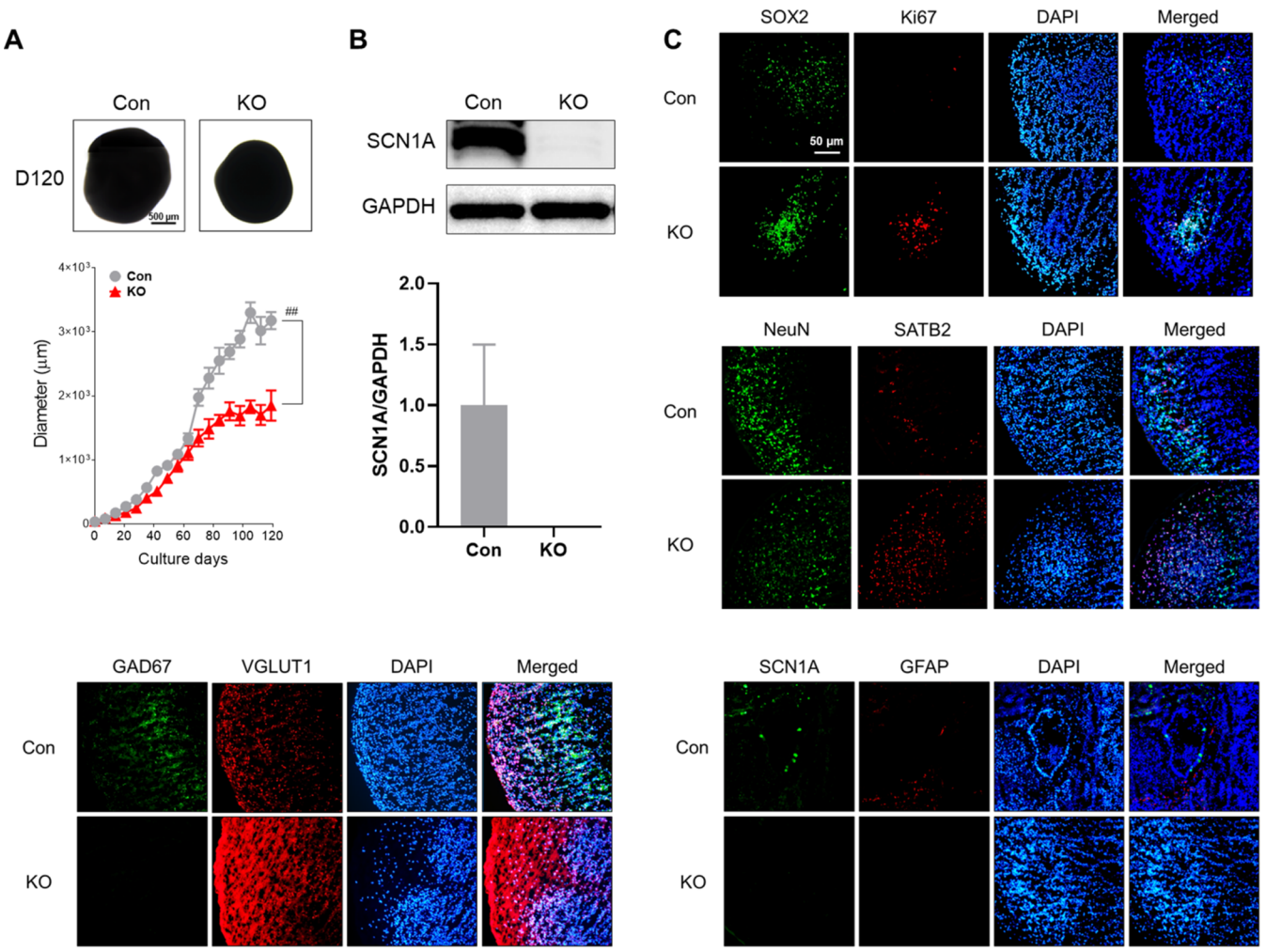

Figure 1. Morphological differences between control (Con) and SCN1A KO (KO) cerebral organoids. (A) Diameter (from 24 individual organoids for each group) (B) 120 days cultured control and SCN1A KO cerebral organoids (from 5 individual organoids for each group) SCN1A protein expression with Western blot and (C) Stem cell and neuronal marker expression of Con vs KO cerebral organoids with immunofluorescence imaging. Error bars represent the standard error of the mean of three independent experiments.

regulation,[16−19] their expression and alterations in recently developed brain organoids remain relatively unexplored. Previous studies utilizing targeted metabolomics, including neurotransmitters and neurosteroids, have provided insights into the dynamic changes occurring during cerebral organoid differentiation.[20] However, there remains a critical gap in understanding, particularly regarding genetic mutations, especially in the context of rare diseases such as SCN1A-associated disorders.

Cerebral organoids, coupled with the multiomics approach, offer an integrated approach to comprehensively analyze molecular components within these structures.[21] This holistic strategy enhances our ability to identify genetic and molecular determinants underlying neurological disorders, paving the way for tailored therapeutic interventions.[22] This study investigates the impact of SCN1A gene knockout (KO) on brain development and function with a multiomics analysis approach using cerebral organoids.

RESULTS

Comparison of Growth and Maturation between Control and SCN1A KO Cerebral Organoids. The diameter of both control and SCN1A KO cerebral organoids was monitored during the culture period. Our data suggest that the diameter of control and SCN1A KO cerebral organoids started to differentiate after 60 days of culture (Figure 1A). After 120 days of culture, the average diameter of control cerebral organoids was about 61.9% larger than that of SCN1A KO organoids (Figure 1A). Western blot data show that the expression of SCN1A protein was not detected in SCN1A KO cerebral organoids after 120 days of culture (Figure 1B). Immunofluorescence images show that the expression levels of the proliferating neuronal marker antigen K_i-67 and the glutamate transport-associated protein Vesicular glutamate transporter 1 (VGLUT1), antigen kiel 67 (K_i-67) were noticeably increased in SCN1A KO cerebral organoids, while the expression level of the GABA synthesis-related Glutamate decarboxylase or glutamic acid decarboxylase 67 (GAD-67), glial fibrillary acidic protein (GFAP) were distinctly decreased compared to that of control cerebral organoids after 120 days of culture (Figure 1C). No significant differences in the expression level of SRY sex determining region Y-box 2 (SOX2), NeuN and special AT-rich sequence-binding protein 2 (SATB2) were detected in SCN1A KO cerebral organoids compare to control.

https://doi.org/10.1021/acsomega.4c05039
ACS Omega 2024, 9, 39804−39816

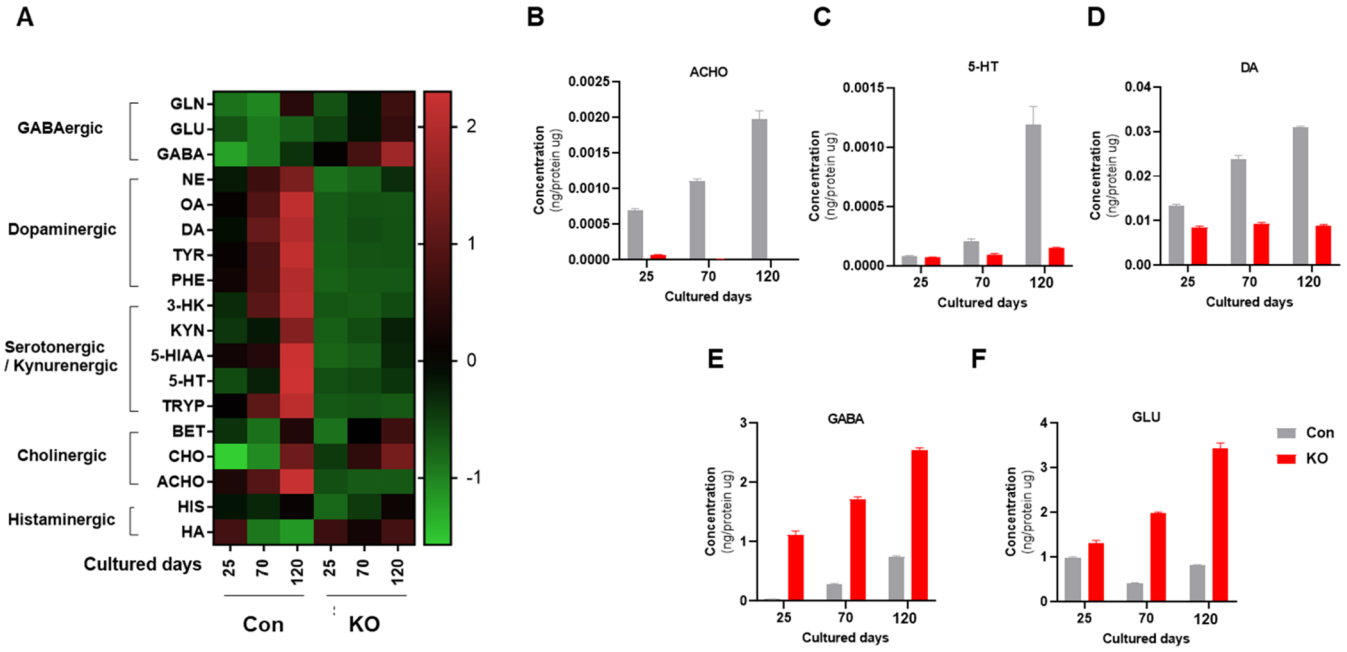

Figure 2. Quantitative analysis of neurotransmitter production by control (Con) and SCN1A KO (KO) cerebral organoids. (A) Heatmap of 18 neurotransmitter production levels. (B) ACHO (C) 5-HT (D) DA (E) GABA and (F) GLU production levels from Con and KO cerebral organoids. Error bars represent the standard error of the mean of three independent experiments.

Dysregulation of Neurotransmitters in Cerebral Organoids. We conducted a quantitative analysis of 18 neurochemicals, encompassing 7 neurotransmitters along with their precursors and metabolites. Figure 2A illustrates the profile change of the 5-categorized neurochemical system in cerebral organoids. The entire data set is standardized using *Z*-scores, with red indicating relative increases and green indicating relative decreases. Overall, the SCN1A KO cerebral organoids exhibited a significantly decreased profile in the overall neurochemical levels compared to the control cerebral organoids. Specifically, significant changes were observed in the cholinergic, serotonergic, kynurenergic, and dopaminergic systems. While the control cerebral organoids showed a significant increase in profile at each developmental stage, the SCN1A KO cerebral organoids, in contrast, displayed limited changes across developmental stages (Figure 2A–D). However, GABAergic neurotransmitters such as GABA and GLU exhibited abnormal increases in SCN1A KO cerebral organoids (Figure 2E,F).

Lipidomic Profiling of Temporal and SCN2A KO-Dependent Alterations. In the present study, we employed partial least-squares-discriminant analysis (PLS-DA) and volcano plot analyses to investigate the lipidomic alterations consequent to the knockout of the SCN1A gene at two distinct time points: Day 0 and Day 120. In the top part of Figure 1A, there are PLS-DA plots revealing the separation between control and SCN1A KO cerebral organoids for Day 0 (top-left) and Day 120 (top-right). These plots highlight the differential clustering of lipid species, signifying a distinct lipidomic profile attributed to the absence of SCN1A gene function. The volcano plots in the lower part of Figure 3A encapsulate the statistical significance against the magnitude of alteration in lipid species between the control and SCN1A KO cerebral organoids for both Day 0 (bottom-left) and Day 120 (bottom-right). The red and blue points represent significantly upregulated and downregulated lipid species, respectively, demonstrating a substantial shift in the lipidome upon the knockout of SCN1A. Changes in identified lipid species are presented as log2 fold change (Log2 FC) values, comparing data from the two time points: Day 0 and Day 120 (Figure 3B). Notably, lipid species such as ether phospholipids (e.g., PC-O 35:1, 35:0, 33:1, and LPC O-19:1, 19:0, 17:0), SM 11:0, and DGCC 18:0 exhibited pronounced alterations in SCN1A KO cerebral organoids following Day 120, underscoring the impact of SCN1A gene knockout on the lipid metabolic pathway.

In our investigation of the lipidomic results of SCN1A gene knockout, we conducted a comprehensive analysis. Figure 3C shows a heatmap of the identified lipid species, which displays the comparative lipid profiles between the control and SCN1A KO cerebral organoids at two different cultivation periods: Day 0 and Day 120. Figure 3D illustrates the log2 fold change (Log2 FC) plot of the identified lipid species, quantifying the magnitude of expression changes between the control and SCN1A KO cerebral organoids at the two time points. Similar to the findings presented in Figure 3B, various ether phospholipids and SM 11:0 showed pronounced upregulation in the SCN1A KO cerebral organoids after 120 days, a pattern that is mirrored in the visualized heatmap.

In our quantitative analysis of neurosteroid changes due to SCN1A gene knockout, Figure 3E illustrates the log2 fold change (Log2 FC) in neurosteroid levels between baseline (Day 0) and an extended period (Day 120) postknockout. The targeted lipidomics assessment was conducted to accurately measure the concentrations of key neurosteroids, including pregnenolone, progesterone, 20α−OH progesterone, cortisol, 11-desoxycortisol, and 21-desoxycortisol. Neurosteroids 11-desoxycortisol and 21-desoxycortisol exhibited substantial upregulation in the SCN1A KO cerebral organoids compared to the control cerebral organoids over the 120-day period. In contrast, pregnenolone and progesterone, along with other metabolites, displayed more modest fluctuations in their levels.

https://doi.org/10.1021/acsomega.4c05039
ACS Omega 2024, 9, 39804−39816

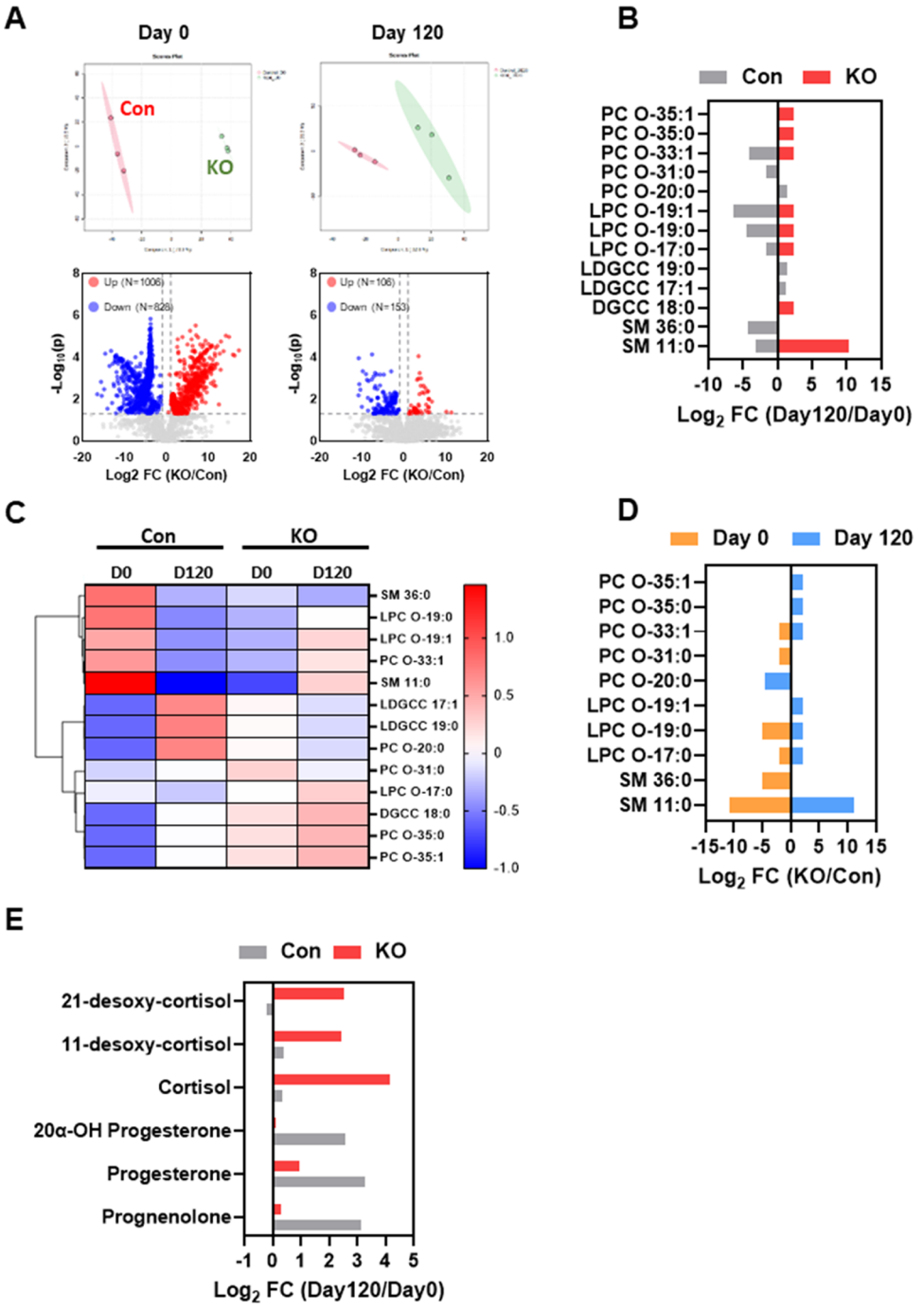

Figure 3. Lipidomics profiling and differential analysis in control (Con) and SCN1A KO (KO) cerebral organoids at Day 0 and after 120 days. (A) Showcases the multivariate and univariate analysis at two time points: PLS-DA plots of day 0 (top-left) and day 120 (top-right) post-SCN1A gene knockout. (B) Log2 fold change (FC) of identified lipid species, comprising day 120 and day 0 for both Con and KO cerebral organoids. (C) Heatmap of the relative abundance of identified lipid species in control and SCN1A gene knockout cerebral organoids at the start (Day 0) and after 120 days (D120) of cultivation. (D) Log2 fold changes of the sample lipid species between the KO and Con cerebral organoids as D0 and D120. (E) Log2 fold change of neurosteroids detected by targeted analysis from Con and KO cerebral organoids at two time points, 0 day and 120 days.

Quantitative Total RNA Sequencing Analysis of Control and SCN1A KO Cerebral Organoids. Total RNA sequencing analysis was conducted for 120 days cultured control and SCN1A KO cerebral organoids (Figure 4A). Among the 30,694 genes detected, the expression level of 1644 genes was increased while the expression level of 1053 was decreased (>2-fold with p-value <0.05) in SCN1A KO cerebral organoids compare to control organoids (Figure 4B,C). Gene Ontology (GO) enrichment analysis suggests that genes related to signaling receptor activity, molecular transducer activity, signal receptor binding activity, cell periphery, and biological regulation were increased in SCN1A KO cerebral organoids compared to those of the control (Figure 4D−F).

Quantitative Proteomic Analysis of Control and SCN1A KO Cerebral Organoids. To explore the differences in protein expression levels between control and SCN1A KO cerebral organoids, we performed quantitative proteomic analysis of SCN1A KO and control cerebral organoids (days

https://doi.org/10.1021/acsomega.4c05039
ACS Omega 2024, 9, 39804−39816

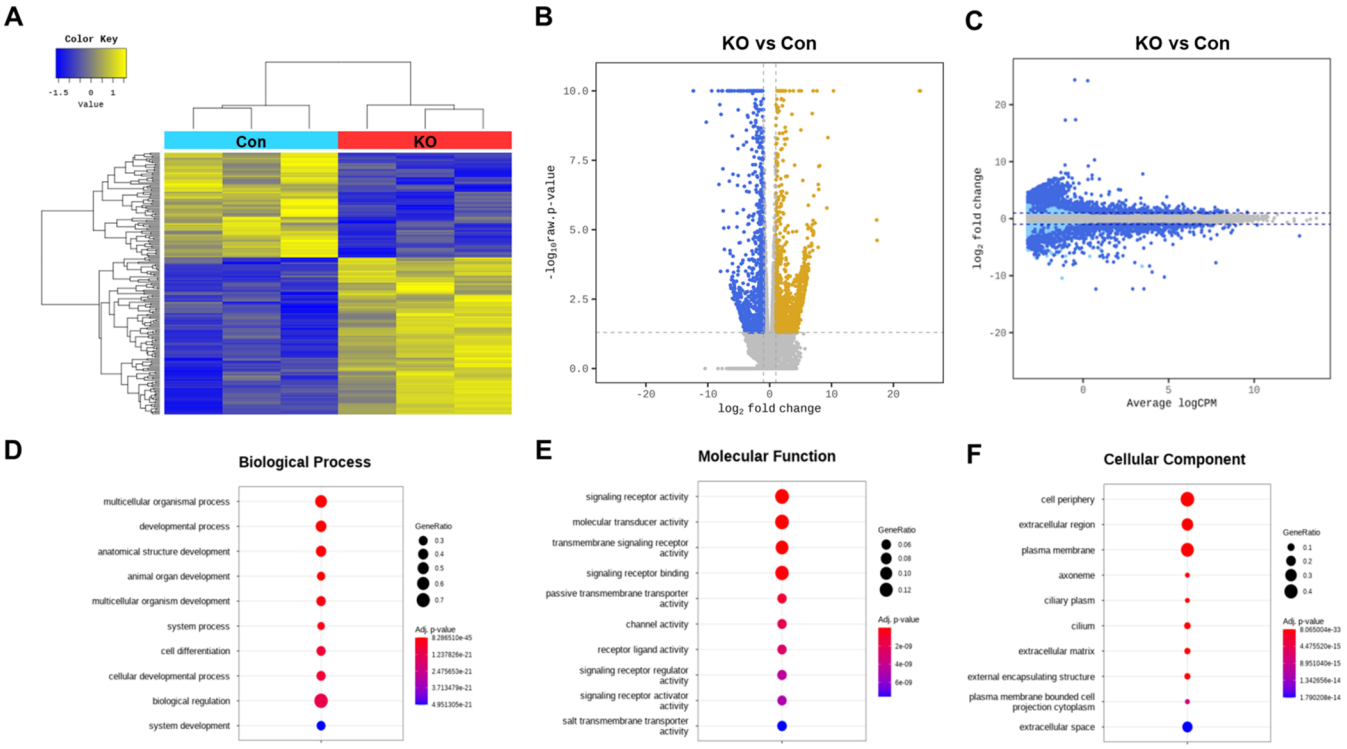

Figure 4. Total RNA sequencing analysis of control (Con) vs SCN1A KO (KO) cerebral organoids. (A) Heatmap, (B) volcano plot, and (C) smear plot of differentially expressed genes (DEGs). Panels (D), (E), and (F) depict gene set enrichment analysis for biological process, molecular function, and cellular component, respectively.

0 and 120) using isobaric tags for relative and absolute quantitation (iTRAQ) coupled with online 2D-nLC-MS/MS. As a result, a total of 5870 proteins, each with at least two peptides and three iTRAQ values, were commonly quantified in both SCN1A KO and control organoids (Supporting Information Tables S1 and S2). Applying a cutoff threshold of a 2-fold change and adjusted p-value <0.05, we identified 14 proteins that were differentially expressed in SCN1A KO organoids compared to controls at day 0 (Figure 5A and Supporting Information Table S1). Functional enrichment analysis using both Gene Ontology (GO) biological process and reactome pathway analysis revealed that downregulated proteins (ACLY, HMGCR, HMGCS1, and FASN) were involved in cholesterol and fatty acid biosynthetic processes (Figure 5B).

Unlike the minimal change in expression levels of differential proteins between control and SCN1A KO organoids at day 0, a total of 286 proteins exhibited significant changes at day 120, with 192/94 proteins up-/downregulated in SCN1A KO organoids compared to controls (Figure 5A and Supporting Information Table S2). Through hierarchical clustering analysis, we categorized the 286 differentially expressed proteins at day 120 into four main clusters based on their expression patterns (Figure 5C and Supporting Information Table S3). In Cluster 1 (62 proteins), the expression levels increased from day 0 to day 120 in controls but showed no significant changes (less than 15%) in SCN1A KO organoids, even from day 0 to day 120 (Figure 5D). Functional enrichment analysis using GO and Reactome pathways revealed that proteins in Cluster 1 were implicated in cholesterol homeostasis, lipid catabolic processes, extracellular matrix organization, and integrin cell surface interactions (Figure 5E).

Cluster 2 contained 27 proteins that showed a slight increase in expression levels from day 0 to day 120 in controls but a slight decrease in SCN1A KO cerebral organoids, with no significant pathway enrichment (less than 17% change). Regarding Cluster 3 (33 proteins), the expression levels increased approximately 2-fold from day 0 to 120 in controls, whereas it showed approximately a 5-fold increase in SCN1A KO cerebral organoids. Additionally, proteins involved in Cluster 4 (150 proteins) were upregulated in both control (approximately 1.5-fold) and SCN1A KO (approximately 2.5-fold) from day 0 to 120. From this in silico proteomic analysis, we found that Clusters 3 and 4 are mainly enriched in proteins associated with the neuronal system, transmission across chemical synapses, regulation of trans-synaptic signaling, synapse organization, salt-dependent response, and sodium ion transport. Relative expression levels of representative sodium ion transporters (SCN2A and SLC1A3) and neuronal proteins (SYN1 and STXBP1) in Clusters 3 and 4 are shown in Figure 5F.

Our global overview suggests that SCN1A KO specifically induces an increase in synaptic vesicle genes/proteins (SYP, SYN1, etc.), clathrin-mediated endocytosis-related genes/proteins, as well as genes/proteins related to the synaptic vesicle cycle (Figure 6).

DISCUSSION

In this study, our aim was to comprehend the distinctions in brain neurochemistry between the control and SCN1A KO cerebral organoids. Several studies have proposed that a thorough quantitative grasp of the broad neurochemical profile reflects alterations in potential behavioral patterns observed in humans.[16−18] The utilization of brain organoids provides diverse advantages as it mimics actual human brain tissue. We

https://doi.org/10.1021/acsomega.4c05039
ACS Omega 2024, 9, 39804−39816

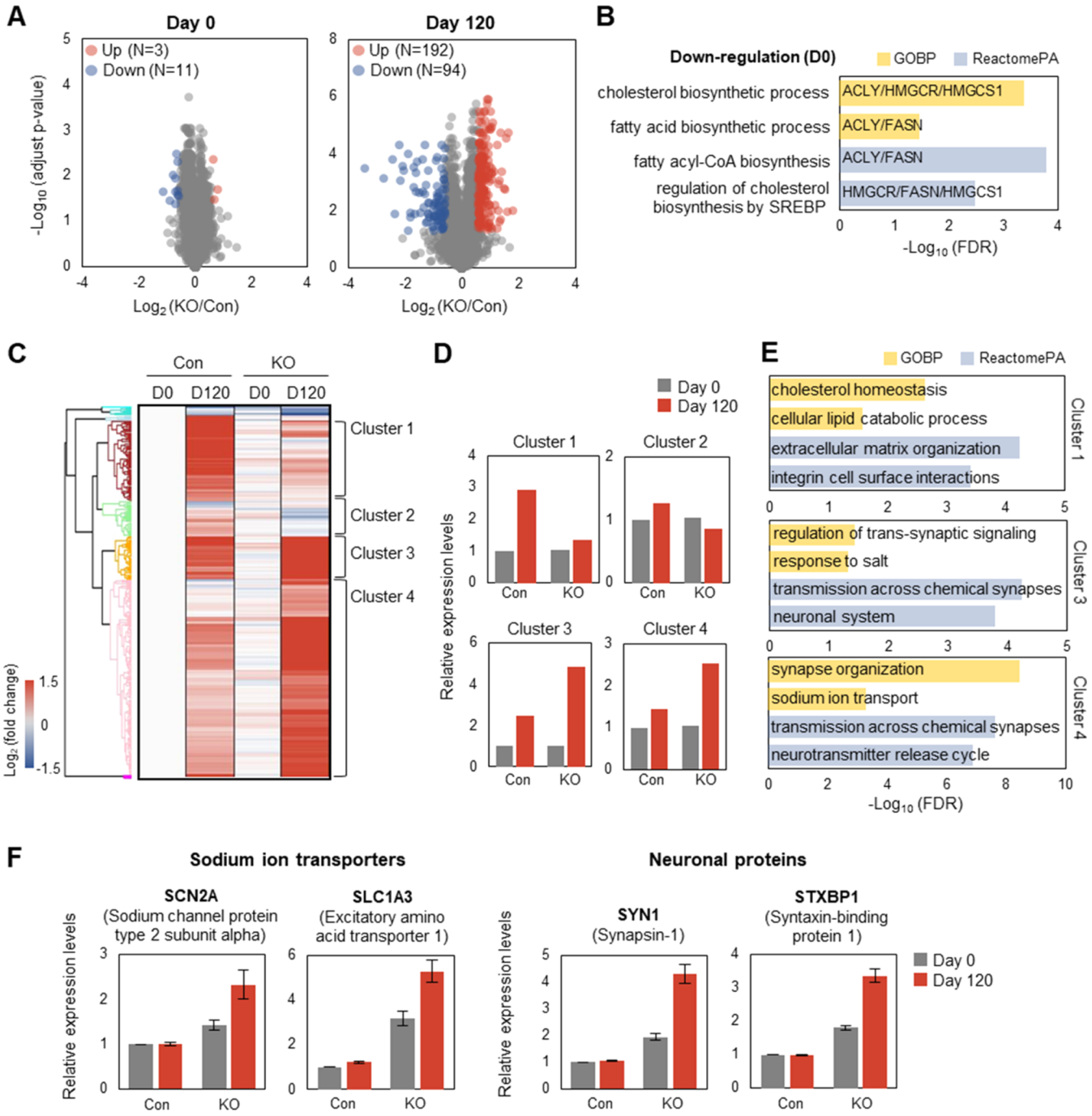

Figure 5. Quantitative proteomic analysis of control (Con) and SCN1A KO (KO) cerebral organoids. (A) Volcano plots displaying log2 fold change (KO/Con) against the −log10 (adjusted p-value) at day 0 (left) and day 120 (right). Red dots represent upregulated proteins, and blue dots represent downregulated proteins. (B) GO annotation and reactome pathway enrichment of downregulated proteins in KO compared with Con cerebral organoids at day 0. (C) Heatmap and hierarchical clustering analysis of differentially expressed proteins between KO and Con cerebral organoids at day 120 (red, high expression; blue, low expression). (D) Average expression levels of proteins in each cluster (Cluster 1, 2, 3, and 4). Gray and red colors indicate day 0 and day 120, respectively. Protein expression levels were normalized to Con cerebral organoids (day 0). (E) GO annotation and reactome pathway enrichment of proteins in Cluster 1, 3, and 4. (F) Relative expression levels of sodium ion transporters (SCN2A and SLC1A3) and neuronal proteins (SYN1 and STXBP1) in Clusters 3 and 4. Error bars represent the standard error of the mean of three independent experiments.

performed quantitative metabolic profiling of various neurochemical systems, including histaminergic, cholinergic, dopaminergic, serotonergic/kynurenergic, and GABAergic, to deepen our understanding of brain neurochemistry in SCN1A KO cerebral organoids. Various neurochemical profiles were dysregulated in SCN1A KO cerebral organoids. More specifically, the SCN1A KO cerebral organoids demonstrated a depletion of ACHO, 5-HT, and DA—key neurotransmitters with crucial roles in the central nervous system associated with learning and memory, sedation, and motor control.[17,23,24] This suggests neurological impairment in the SCN1A KO cerebral organoids, particularly concerning

https://doi.org/10.1021/acsomega.4c05039
ACS Omega 2024, 9, 39804−39816

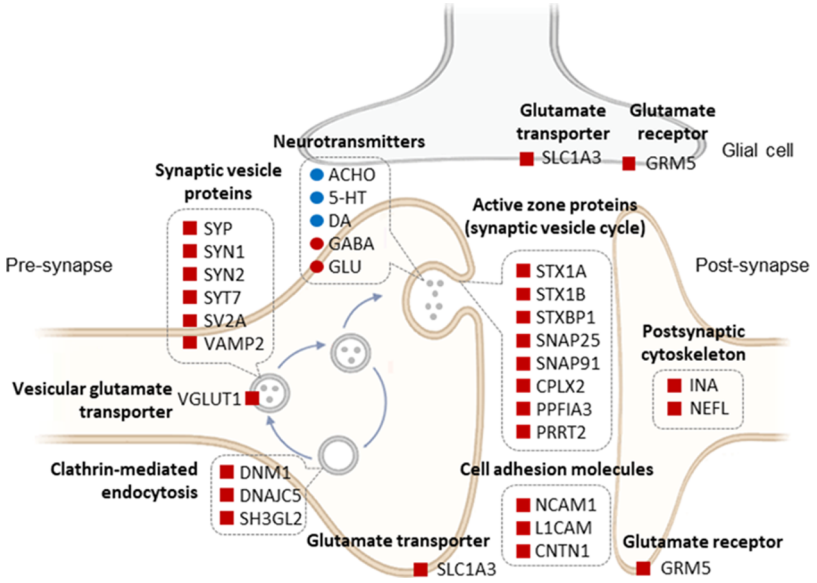

Figure 6. Regulation of synaptic proteins and neurotransmitters in SCN1A KO cerebral organoids. Red and blue colors represent up- and downregulation in SCN1A KO organoids compared to control at day 120, respectively. Dots indicate neurotransmitters, and squares indicate proteins.

neurochemical synthesis during brain development. ACHO, a neurotransmitter, is synthesized from CHO through the action of the metabolic enzyme choline acetyltransferase (ChAT) and is associated with diverse neurological disorders. In Alzheimer's disease, ACHO plays a pivotal role in cognitive function and memory. The pathology of Alzheimer's disease involves a significant reduction in ACHO levels in the brain, leading to impaired neurotransmission and cognitive decline.[16,25] Moreover, 5-HT is produced from the amino acid TRYP by Tryptophan dehydroxylase (TPH) and amino acid decarboxylase (AADC) in brain tissue, playing a regulatory role in mood and sleep patterns. Insufficient 5-HT levels have been associated with depressive manifestations, including feelings of sadness and reduced interest, while disruptions in 5-HT function are implicated in sleep disorders such as insomnia.[26] Additionally, decreased 5-HT levels have been observed in chemically or genetically induced epileptic seizure models, attributed to the depletion of serotonin's sedating effect.[27,28] Serotonin also prevents seizure behavior, indicating a molecular linkage between 5-HT and epilepsy. GABA is derived from the amino acid GLU through the action of the enzyme glutamate decarboxylase (GDC) in neurons. However, the current study observed a notable increase in both GABA and GLU levels in the SCN1A KO cerebral organoids, indicating significant abnormal changes in synaptic plasticity. These alterations suggest potential abnormalities in neural activity within the nervous system, implying potential repercussions on neurological function.[29] In a recent study, it was demonstrated that mouse models with SCN1A KO and SCN1B KO mutations, which are associated with Dravet Syndrome, exhibit immature GABAergic signaling, potentially contributing to epileptogenesis.[30] Additionally, SCN1A KO mice exhibited periodic generalized clonic and bilateral forelimb convulsive seizures with a specific loss of sodium current in GABAergic interneurons in the hippocampus of SCN1A ± and SCN1A KO mice.[31]

These outcomes could contribute to the worsening of seizures, status epilepticus, and Sudden Unexpected Deaths in Epilepsy (SUDEP) in Dravet syndrome patients. However, the physiological relationship between neurotransmitter levels, including ACHO, 5-HT, GABA, and GLU, and the epileptogenic potential in humans remains unclear. We acknowledge that the results of neurotransmitter analysis in brain organoids do not claim to perfectly replicate actual human neurochemistry. Nevertheless, integrating neurochemical analysis results from brain organoids with various omics data will offer a synergistic insight, aiding in the anticipation of potential changes in actual humans. Therefore, we further analyzed a multiomics approach to gain a better understanding of the disease status of SCN1A KO through lipidomic, proteomic, and transcriptomic approaches.

Lipids play an essential and multifaceted role in brain function and structure. They are not only major components of the cellular membranes that encase neurons and glial cells but also serve as signaling molecules, energy homeostasis, and modulators of protein function.[32−34] Disruption of lipid homeostasis can lead to altered membrane properties, impaired energy metabolism, dysfunctional signaling pathways, and neurogenic disorders.[35,36] Our nontargeted lipidomic results reveal dynamic alterations in lipid profiles that may support the neurological manifestations of Dravet syndrome. At baseline (Day 0), our control and SCN1A KO cerebral organoids showed distinct lipidomic profiles, indicating that even in the absence of overt phenotypic expression, molecular differences are already present. Notably, levels of specific ether phospholipids in the knockout model were increased. Ether phospholipids also play vital roles in neuropsychiatric disorders' brain function, pathology, and protection from oxidative stress.[37,38] In most previous studies addressing brain diseases, it has been reported that the deficiency of ether phospholipids, such as plasmalogen, contributes to the induction of these diseases due to increased oxidative stress.[37,39,40] While a limited number of studies have reported an increase in plasmalogen levels in the brain, our results suggest that this elevation might represent a negative feedback response to increased oxidative stress or could be due to overproduction associated with peroxisome dysfunction. A significant increase in the levels of SM 11:0, a lipid species of

https://doi.org/10.1021/acsomega.4c05039
ACS Omega 2024, 9, 39804−39816

sphingomyelin, was observed in the present study. Sphingomyelin is related to neuronal excitability. Sphingomyelin present in the plasma membrane can be cleaved by neutral sphingomyelinases (nSMase), generating ceramides and sphingosine-1-phosphate (S1P), which are known to contribute to neuronal excitability.[41] This neural excitability can lead to recurrent epileptic seizures.[42] Although the activity of nSMase was not measured in our study, the elevated levels of sphingomyelin observed in the KO cerebral organoids at 120 days suggest the possibility of its hydrolysis, potentially contributing to increased neuronal excitability. Neurosteroids are brain-synthesized steroids that modulate brain activity by enhancing inhibitory neurotransmission and relaxing excitatory responses, playing a key role in maintaining neural function and offering potential therapeutic targets for various neurological disorders disorders.[43,44] In the SCN1A KO cerebral organoids at 120 days, there was a trend of increased levels of pregnenolone and its metabolite, progesterone, and 20α-OH progesterone, though these levels were lower compared to the control cerebral organoids at the same time point. This pattern suggests an upregulating of the corresponding biosynthetic pathway or a downregulation of their further metabolism. The diminished levels of pregnenolone and its metabolites observed in the 120-day SCN1A KO cerebral organoids might be associated with the brain's neuroprotective response to epileptic activity, given that pregnenolone and its metabolites have demonstrated anticonvulsant effect.[45,46] Conversely, the stress-related corticosteroids, cortisol and its precursors, 11-desoxycortisol, and 21-desoxycortisol, were also elevated, reflecting a possible chronic stress response in the 120-day SCN1A KO cerebral organoids.[47] This pattern of hormonal changes is consistent with reports showing increased seizure frequency due to stress responses.[45]

In the quantitative proteomic analysis of control and SCN1A KO organoids, we observed dysregulation of proteins associated with cholesterol metabolism in SCN1A KO cerebral organoids. Compared with control cerebral organoids, the expression levels of proteins (ACLY, HMGCR, HMGCS1, and FASN) that play an important role in cholesterol/fatty acid synthesis were decreased in SCN1A KO at day 0. Additionally, proteins (APOA1, APOA4, APOB, MTTP, and EPHX2) involved in cholesterol homeostasis were upregulated in control but not in SCN1A KO during neuronal differentiation of organoids. Cholesterol is a major component of cellular membranes and a precursor molecule of steroid hormones, playing essential roles in neuronal physiology.[48] Therefore, the impairment of cholesterol metabolism may contribute to neuronal dysfunction in SCN1A KO cerebral organoids. Our proteomic study also revealed an upregulation of various sodium ion transporters (SCN2A, ATP1A3, ATP1B1, SLC9A6, SLC8A1, SLC3A1, SLC1A3, SLC6A17, and SLC23A2) in SCN1A KO organoids compared with control at day 120. Notably, in addition to the neuronal voltage-gated sodium channel NaV1.2 (SCN2A), the excitatory amino acid transporter 1 (SLC1A3) was upregulated in SCN1A KO organoids at day 120. SLC1A3 is a glutamate transporter that uptakes glutamate released from the synaptic cleft, which is crucial in the termination of synaptic transmission at excitatory synapses. Therefore, upregulation of SLC1A3 could potentially affect abnormal synaptic transmission in SCN1A KO cerebral organoids. Furthermore, our study demonstrated the upregulation of numerous neuronal proteins, including synaptic proteins SYN1 and STXBP1, in SCN1A KO organoids compared with control at day 120. Taken together, these proteomic findings suggest that the disruption of SCN1A may lead to the dysregulation of proteins involved in sodium ion transport and neuronal functions, resulting in neural abnormalities.

In the Transcriptome/Proteome analysis, we focused on genes/proteins with a *P*-value less than 0.05. (For the Transcriptome, we used the FC and p-value obtained from the Lead count values provided by Macrogen for the analysis.) As a result, only 334 genes/proteins were analyzed in both the Transcriptome and Proteome, which was fewer than expected (Figure S1). Additionally, when we plotted the Fold change values on a graph, it showed an *R* value of 0.049, indicating no correlation between the data.

Of note, we used cerebral organoids derived from unmodified IMR90-4 as a control when comparing multiomics profiles with SCN1A KO IMR90-4 derived cerebral organoids. Previous studies have shown that nonspecific effects of molecular alterations or cellular stress can be induced during transfection with CRISPR-Cas9.[49,50] Therefore, it is important to set proper controls and carefully examine the effects of genetic modification during the CRISPR-Cas9 knockout procedure, as it may influence the studied system.

In summary, we conducted a systematic comparison of control vs SCN1A KO cerebral organoids using a multiomics analysis approach. Our data reveal differences in neurotransmitter, neurosteroid/lipid, RNA, and protein expression in SCN1A KO cerebral organoids compared to control. These findings may contribute to our understanding of Dravet syndrome and aid in future treatment development.

METHODS

Generation of SCN1A KO-Induced Pluripotent Stem Cell Lines. Induced pluripotent stem cells (iPSCs) derived from IMR90-4 cells {iPS(IMR90)-4, obtained from WiCell, Madison, WI} were subjected to SCN1A KO using the CRISPR-Cas9 system by Toolgen, Inc. (Seoul, Korea). The following gRNA sequences were used for SCN1A knockout: 5′-CAAACAGTGCTTGTACCACC-3′ (5′ gRNA) and 5′-TCGTCGTCATCTTTTTTGTCTGG-3′ (3′ gRNA). The gene knockout protocol employed the NEON system for electroporation of a DNA mixture containing two pX330 plasmids encoding Cas9 and gRNA. Electroporation was conducted following the manufacturer's instructions. In brief, 3 mL of the electrolytic buffer was inserted into the Neon pipet station. Plasmid DNA/siRNA with cells in a microcentrifuge tube was loaded, and the electroporation process was started. Enzymes were used to generate cohesive ends (sticky ends) on the DNA coding for the selection marker. The transfected cells were then cultured under antibiotic selection for 5 days. Following selection, cells maintaining morphology under the highest antibiotic concentration were reseeded and cultured for 8 days in the presence of multiple antibiotics. Sanger sequencing results of SCN1A KO iPSCs can be found in Supporting Information sequence trail files.

Cerebral Organoid Culture. Cerebral organoids were grown and developed over a span exceeding 120 days following a previously established protocol with minor adjustments.[20,51] Control (iPS(IMR90)-4) and SCN1A KO iPS(IMR90)-4 were initially seeded onto a 6-well cell culture plate (Corning, Corning, NY) precoated with matrigel (Corning) diluted 120 times in Dulbecco's modified Eagle medium/nutrient mixture F-12 (DMEM/F-12, Invitrogen, Carlsbad, CA). Starting from

https://doi.org/10.1021/acsomega.4c05039
ACS Omega 2024, 9, 39804−39816

day 0, the iPS(IMR90)-4 cells were cultured in mTeSR1 medium (Stem cell technologies, Vancouver, Canada) supplemented with 1 μM Y-27632 (Tocris, Bristol, UK). Subsequently, the medium was replaced daily with Y-27632-free mTeSR1 from day 1 onward. To initiate the formation of cerebral organoids, 2×10^4 iPS(IMR90)-4 cells were seeded into each well of a U-bottom ultralow-attachment 96-well plate (Corning) in neural induction media. This media comprised DMEM/F-12 supplemented with 1% glutanax, 1% minimum essential medium-non essential amino acids (MEM-NEAA), 15% knockout serum, 0.1 nM β-mercaptoethanol, 100 nM LDN-193189 (Sigma-Aldrich, St. Louis, MO), 10 μM SB431542 (Sigma-Aldrich), and 2 μM XAV939 (Sigma-Aldrich). The cells were then cultured for 10 days, with media changes performed every other day. Following the initial static culture period, the cerebral organoids were transferred to ultralow-attachment 6-well plates (Corning) for further development in neural differentiation media. This media consisted of a mixture of DMEM/F12 and neurobasal media (Corning) supplemented with N2 and B27 supplements (without vitamin A, Thermo Fisher Scientific, Waltham, MA), 1% MEM-NEAA (Thermo Fisher Scientific), 1% GlutaMAX (Thermo Fisher Scientific), and human insulin solution (Thermo Fisher Scientific). The cells were cultured for an additional 8 days with orbital shaking at 80 rpm/min. For the subsequent neural maturation phase of the cerebral organoids, the media was switched to neural differentiation media containing B27 supplement with vitamin A, brain-derived neurotrophic factor (BDNF), cyclic adenosine monophosphate (cAMP), and ascorbic acid, with media changes performed every 4 days starting from day 18.

Immunohistochemistry. Cerebral organoids underwent a washing step with 500 μL of Dulbecco's phosphate-buffered saline (DPBS, Thermo Fisher Scientific). Subsequently, the organoids were fixed overnight by incubating them with 4% paraformaldehyde (PFA, Sigma−Aldrich). After fixation, the organoids underwent two washes with DPBS and were then sequentially immersed in 10, 20, and 30% sucrose solutions to enhance their density for easier sectioning. Cryoblocks of the organoids were formed using an optimal cutting temperature (OCT, Sakura Finetech USA, Inc., Torrance, CA) compound. These cryoblocks were frozen both prior to and after embedding in OCT to ensure uniform freezing of the organoids. The cryosections were then washed with DPBS to eliminate excess OCT and were blocked in a solution containing 1% bovine serum albumin (BSA, Sigma−Aldrich) and 0.1% Triton X-100 diluted in DPBS for 1 h at room temperature. This blocking step aimed to minimize nonspecific binding of primary antibodies. Following blocking, the sections were incubated overnight at 4 °C with primary antibodies, diluted in a solution containing 1% BSA and 0.1% Triton X-100. The primary antibodies used for immunofluorescence labeling included SOX2 (Abcam, Cambridge, UK), Ki67 (Cell Signaling Technology, CST, Danvers, MA), GFAP (CST), NeuN (CST), SCN1A (CST), GAD67 (CST), SATB2 (CST), and VGLUT1 (CST). After incubation with primary antibodies, any unbound antibodies were washed away using DPBS, and the cryosections were then incubated with secondary antibodies (Goat anti-Rabbit, Goat anti-Mouse, Thermo Fisher Scientific) containing 2% normal goat serum (NGS) and 0.1% Triton X-100 for 1 h. These secondary antibodies were conjugated to Alexa Fluor dyes (488, 594) to enhance signal detection. Finally, nuclei were stained with 4′,6-diamidino-2-phenylindole (DAPI, Thermo Fisher Scientific, Inc.) to visualize them under fluorescence microscopy.

Neurotransmitter Analysis. The quantitative analysis of 18 neurochemicals, including histamine (HIS), histamine (HA) in histaminergic systems, acetylcholine (ACHO), choline (CHO), betaine (BET) in the cholinergic system, tryptophan (TRYP), serotonin (5-HT), 5-hydroxyindole acetic acid (5-HIAA), kynurenine (KYN), 3-hydroxy kynurenine (3-HK) in serotonergic/kynurenergic systems, phenylalanine (PHE), tyrosine (TYR), dopamine (DA), octopamine (OA), norepinephrine (NE) in the dopaminergic system, and γ-aminobutyric acid (GABA), glutamate (GLU), and glutamine (GLN) in the GABAergic system, was performed using ultraperformance liquid chromatography (UPLC) coupled with a Xevo TQ-S triple quadrupole mass spectrometer (MS). The analysis followed a previously documented method.[52] Cerebral organoids underwent several procedures, including three washes with 0.1 M phosphate-buffered saline (pH 7.4), addition to distilled water with 1% formic acid (FA), homogenization via a probe-type sonicator, and centrifugation at 15,000 rpm for 20 min at 4 °C. The protein concentration (μg/μL) in each supernatant was measured using a BCA protein assay (Thermo Scientific) to normalize the concentration of the 18 neurotransmitters, determined through LC−MS/MS analysis. The final concentration of neurotransmitters was either converted to a log2 scale for comparison of fold change or standardized by Z-score, representing the number of standard deviations a data point is from the mean. The formula for calculating the Z-score is

$$Z\text{-score} = \frac{(X - \mu)}{\sigma}$$

where X is the raw data (neurotransmitter concentration/protein concentration), μ/μ is the mean of the data set, and σ/σ is the standard deviation of the data set. The resulting supernatant underwent extraction by mixing with an equal volume of methanol containing 1% FA and an isotope-labeled internal standard, followed by vortexing and centrifugation at 15,000 rpm for 10 min at 4 °C. The clear supernatant obtained was transferred to LC vials for subsequent analysis. The concentrations of the 18 neurotransmitters were normalized based on the protein content of the organoid homogenate, determined through LC−MS/MS analysis. Three biological replicates were prepared for each condition.

Metabolic Profiling. For metabolic profiling in cerebral organoid, UPLC-Q-TOF-MS analysis was performed using Waters ACQUITY UPLC system (Waters Corporation, Milford, MA) coupled to a Waters Xevo Q-TOF mass spectrometry (Waters corporation) with both electrospray ionization (ESI) positive (ESI+) and negative (ESI-) modes. Sample preparation for metabolites extraction from cerebral organoids was carried out with modification based on previously published protocol.[53] Briefly, medium was removed by Kimtech science wiper. Metabolite extraction was performed by ice-cold methanol. Methanol was added in sample tube followed it was sonicated for 10 min. Then the sample was incubated for 1 h at room temperature. After vortex mixing it is centrifuged at 13,500 rpm for 10 min. Supernatant was separated from sample pellet then transferred another tube and evaporated under nitrogen gas. The extracts were reconstituted in 200 μL of 10% methanol. The sample was transferred into LC vial for UPLC-Q-TOF-MS analysis. Three biological replicates were prepared for each condition.

https://doi.org/10.1021/acsomega.4c05039
ACS Omega 2024, 9, 39804−39816

Metabolic Profiling Data Processing and Identification. The acquired spectral data files of both ESI positive and negative (.raw Waters) were converted to. ABF format using Reifycs Analysis Base File Converter (Reifycs Inc., Tokyo, Japan) using default settings and then processed using MS-DIAL software version 5.1.2.[10] Feature detection, spectra deconvolution, lipid identification, and peak alignment among samples were conducted using MS-DIAL software. MS/MS spectra-based lipid identification was performed in MS-DIAL software by searching the acquired MS/MS spectra against the internal *in silico* MS/MS spectra database. The resulting three-dimensional data comprised of peak number (RT − m/z pair), and ion intensity. The data matrixes of samples with detected features and corresponding three-dimensional value (RT, m/z, and intensity) were produced and imported to Metaboanalyst 5.0 (http://www.metaboanalyst.ca/) for multivariate data analysis.

Multivariate Metabolic Profiling Data Analysis. The data matrixes were rearranged by data format of Metaboanalyst, and saved with. CSV file. The metabolite data were normalized by median normalization, were log transformed, and were auto scaled before multivariate analysis. To evaluate the normality of the data set, the Kolmogorov−Smirnov (K−S) test was applied for all metabolite features (the null hypothesis is that the distribution does not deviate from a normal distribution; $P < 0.05$ indicate a deviation from normality). Given the large size data set, the Shapiro-Wilk test was not appropriate, so we selected the K−S test instead. The results demonstrated that the data did not follow a normal distribution ($P < 0.05$). Therefore, we used the Mann−Whitney U test to analyze the non-normal data, as it is a suitable nonparametric test for comparing differences between two independent groups. The Mann−Whitney U test results confirmed statistically significant differences between the groups ($P < 0.05$). These statistical analyses were carried out using the "scipy" library in the PyCharm Community Edition (ver. 2023.2.3) environment. Principal component analysis (PCA), partial least-squares-discriminant analysis (PLS-DA), one-way analysis of variance (ANOVA) and production of volcano plot were performed by Metaboanalyst algorithm. The PLS-DA model was evaluated by cross-validation text using parameters R^2 and Q^2. To compare each metabolite feature, one-way ANOVA was also performed. Significantly changed metabolites were identified with a threshold of variable importance in the projection (VIP > 1) from the PLS-DA analysis, 2-fold change and p-value controlled the false discovery rate (FDR < 0.05).

Total RNA Sequencing. The Quant-IT RiboGreen assay (Invitrogen, #R11490) was employed to determine the total RNA concentration. Subsequently, the integrity of the total RNA was evaluated by analyzing the samples on the TapeStation RNA screentape (Agilent Technologies, Waldbronn, Germany). RNA isolation from each sample was carried out, and sequencing libraries were constructed using the SMARTer Universal Low Input RNA Kit for Sequencing, adhering to the manufacturer's protocol. Following rRNA depletion, first-strand cDNA synthesis was initiated with the SMART N6 CDS Primer, utilizing the SMARTer II An Oligonucleotide for template switching at the 5′ end of the transcript. The selectively bound first-strand cDNA was separated from contaminants through magnetic separation with SPRI beads. The beads, carrying the purified cDNA, were directly employed for PCR amplification, using the Advantage 2 Polymerase Mix for long-distance PCR. The PCR-amplified cDNA underwent purification via immobilization on AMPure XP beads, followed by washing with 80% ethanol, and elution with elution buffer. Before generating the final library for Illumina sequencing, the amplified cDNA underwent digestion with RsaI to eliminate the SMART adapter. The resulting cDNA fragments underwent end repair, addition of a single 'A' base, and ligation of the indexing adapters. The products were then subjected to purification and enrichment through PCR to form the ultimate cDNA library. Quantification of the libraries was carried out using qPCR following the qPCR Quantification Protocol Guide (KAPA Library Quantification kits for Illumina Sequencing platforms), and their quality was assessed using the Agilent Technologies 4200 TapeStation. Indexed libraries were subsequently sequenced on the NovaSeq platform (Illumina, San Diego, CA) by Macrogen Incorporated (Seoul, Korea). Three biological replicates were prepared for each condition.

Process of mRNA Sequencing. The raw reads obtained from the sequencer underwent preprocessing to eliminate low-quality sequences and adapter contaminants. Subsequently, the processed reads were aligned to the *Homo sapiens* (GRCh37) reference genome using HISAT v2.1.0. HISAT utilizes both global whole-genome indexes and numerous small local indexes, constructed using the efficient Burrows−Wheeler transform (BWT) and graph FM index (GFM) similar to Bowtie2. This approach enables HISAT to achieve spliced alignments significantly faster than Bowtie and BWA. The reference genome sequence and annotation data for *Homo sapiens* (GRCh37) were acquired from NCBI. Following alignment, StringTie v2.1.3b was employed to assemble the aligned reads into transcripts and estimate their abundance. This provided relative abundance estimates in terms of read count values for transcripts and genes expressed in each sample. Library preparation utilized the SMARTer universal low RNA library (Ribo-Zero) kit, and paired-end sequencing reads of 101 base pairs generated from Illumina instruments were assessed for sequence quality using FastQC (version 0.11.7). Prior to analysis, Trimmomatic (version 0.38) was employed to remove adapter sequences and bases with a base quality lower than 3 from the end reads. Additionally, using the sliding window trim method, bases not meeting the criteria of window size = 4 and mean quality = 15 were trimmed. Subsequently, reads shorter than 36 base pairs were filtered out to produce clean data for downstream analysis.

Sample Preparation for Proteomic Analysis. The preparation of cerebral organoids for proteomic analysis followed previously described procedures.[20] In brief, organoid pellets were resuspended in lysis buffer [75 mM NaCl, 8 M urea, 50 mM Tris-HCl (pH 8.0), and protease inhibitors] and homogenized using an ultrasonic homogenizer (Omni, Kennesaw, GA). The remaining cell debris was removed by centrifugation at 14,000g for 15 min at 4 °C, and the resulting supernatant was collected for further analysis. The protein concentration of each sample was assessed by a bicinchoninic acid (BCA) assay. An equal amount of protein (50 μg) from each sample was reduced with 10 mM dithiothreitol (DTT) for 2 h at 37 °C and alkylated with 20 mM iodoacetamide (IAA) for 30 min at room temperature, followed by quenching with 20 mM L-cysteine. The samples were diluted to a final concentration of 1 M urea using 50 mM ammonium bicarbonate buffer and further subjected to digestion with trypsin (enzyme to protein ratio of 1:50) at 37 °C for 18 h.

https://doi.org/10.1021/acsomega.4c05039
ACS Omega 2024, 9, 39804−39816

The resulting peptides were desalted using an OASIS HLB cartridge (Waters Corporation, Milford, MA), and dried in a vacuum concentrator (HyperVAC-LITE, Gyrozen, Rep. of Korea). The tryptic peptides were labeled using 8-plex iTRAQ reagents (AB Sciex) in accordance with the manufacturer's instructions. After desalting with an OASIS HLB cartridge, the labeled peptides were subjected to two-dimensional nanoflow liquid chromatography-tandem mass spectrometry (2D-nLC-MS/MS) analysis. Three biological replicates were prepared for each condition, and each biological replicate was analyzed by 2D-nLC-MS/MS with triplicate runs.

Online 2D-nLC-MS/MS Analysis. The online 2D-nLC-MS/MS was carried out by coupling Agilent 1290 infinity capillary LC system (Agilent Technologies, Santa Clara, CA) with Q-Exactive Hybrid-Quadrupole-Orbitrap MS (Thermo Fisher Scientific, Inc.). The iTRAQ-labeled peptides were loaded onto a biphasic trap column (40 mm in length, 200-μm I.D) packed with 5 mm of reverse-phase (RP) C18 resin (5 μm-200 Å), followed by 15 mm of SCX resin (5 μm-200 Å). The trapped peptides were eluted from the SCX resin to the next RP resin of a biphasic trap column using 12-step gradients of increasing salt concentration (18, 20, 22, 24, 26, 28, 30, 35, 50, 80, 100, and 1000 ammonium bicarbonate) and subsequently separated on an RP column (150 cm in length, 75 μm I.D) packed with C18 resin (3 μm-100 Å) at a flow rate 200 nL/min for 120 min. The MS operated in a data-dependent mode. Full-scan MS data were collected in a scan range of 300 to 1800 m/z with a resolution of 70,000, an automatic gain control target value of 3×10^6, and dynamic exclusion duration of 30 s. The 12 most abundant precursor ions were selected for MS/MS fragmentation. MS/MS spectra were acquired at a resolution of 35,000 with a starting mass of 100 m/z. The normalized collision energy was set to 27%.

Proteomic Data Analysis. All MS raw data files were analyzed using MaxQuant software (version 1.6.6.0) with the Andromeda search engine against a database of UniProt *Homo sapiens* database (release version of Mar 2021 containing 78,120 entries).[54] The search type was set to "Reporter ion MS2" with 8-plex iTRAQ for isobaric label quantification. Trypsin was selected as the enzyme, allowing for maximum of two missed cleavages. The mass tolerance for precursor ions was 4.5 ppm and for the fragment ions was 20 ppm. The 1% false discovery rate (FDR) was applied at both the protein and peptide levels. Carbamidomethylation of cysteine was set as a fixed modification, methionine oxidation and N-terminal acetylation were chosen as variable modifications. Data were filtered for potential contaminants, reverse hits, and proteins only identified by site. Only proteins identified by at least two unique peptides were used for further analysis. Statistical analyses were performed using the Perseus software (version 1.6.14.0).[55] The iTRAQ ratios were $\log_2$ transformed and subsequently normalized by median subtraction. Proteins quantified in at least three out of nine replicates were considered for the analysis. Student's t test and multiple-sample test (one-way ANOVA) were used to determine significance. All P-values were adjusted for multiple hypothesis testing using the Benjamini–Hochberg correction. Hierarchical clustering was also performed using the Perseus software. Functional annotation of Gene Ontology (GO) and enrichment of reactome pathway were conducted in R (version 4.3.1) using the Bioconductor (version 3.17).

Statistical Analysis. Statistical analysis was performed using GraphPad Prism 9 software (GraphPad Software, San Diego, CA) and Origin 8.5 (OriginLab Corporation, Northampton, MA). The values are expressed as the mean ± standard error of means (SEM). The statistical significance was determined by Student's t test for independent samples or one-way ANOVA with Tukey's multiple comparisons. Statistical significance was considered at $^{\#}P < 0.05$, $^{\#\#}P < 0.01$, $^{\#\#\#}P < 0.001$.

■ ASSOCIATED CONTENT

Data Availability Statement

The MS-based proteomic data sets generated during the current study are available in PRIDE, accession number: PDX049155 (http://www.ebi.ac.uk/pride/archive/login).

Supporting Information

The Supporting Information is available free of charge at https://pubs.acs.org/doi/10.1021/acsomega.4c05039.

> Integration of transcriptome and proteomics data, list of all the proteins quantified in SCN1A-KO and WT cerebral organoids at day 0, list of all the proteins quantified in SCN1A-KO and WT cerebral organoids at day 120, summary of hierarchical clustering analysis of differentially expressed proteins between SCN1A-KO and WT organoids at day 120, integration of transcriptomic and proteomic data (PDF)

■ AUTHOR INFORMATION

Corresponding Authors

Sung-Hee Cho − *Chemical Platform Technology Division, Korea Research Institute of Chemical Technology (KRICT), Daejeon 34114, Republic of Korea*; Email: shc0429@krict.re.kr

Myung Ae Bae − *Therapeutics and Biotechnology Division, Korea Research Institute of Chemical Technology (KRICT), Daejeon 34114, Republic of Korea*; Email: mbae@krict.re.kr

Dukjin Kang − *Group for Biometrology, Korea Research Institute of Standards and Science (KRISS), Daejeon 34113, Republic of Korea*; Email: djkang@kriss.re.kr

Ki Young Kim − *Therapeutics and Biotechnology Division, Korea Research Institute of Chemical Technology (KRICT), Daejeon 34114, Republic of Korea*; Email: kykim@krict.re.kr

Authors

Byumseok Koh − *Therapeutics and Biotechnology Division, Korea Research Institute of Chemical Technology (KRICT), Daejeon 34114, Republic of Korea*; orcid.org/0000-0002-1106-1891

Young Eun Kim − *Group for Biometrology, Korea Research Institute of Standards and Science (KRISS), Daejeon 34113, Republic of Korea; School of Earth Sciences & Environmental Engineering, Gwangju Institute of Science and Technology (GIST), Gwangju 61005, Republic of Korea*

Sung Bum Park − *Therapeutics and Biotechnology Division, Korea Research Institute of Chemical Technology (KRICT), Daejeon 34114, Republic of Korea*

Seong Soon Kim − *Therapeutics and Biotechnology Division, Korea Research Institute of Chemical Technology (KRICT), Daejeon 34114, Republic of Korea*; orcid.org/0000-0002-4762-8693

Jangjae Lee − *Chemical Platform Technology Division, Korea Research Institute of Chemical Technology (KRICT),*

https://doi.org/10.1021/acsomega.4c05039
ACS Omega 2024, 9, 39804−39816

Daejeon 34114, Republic of Korea; Department of Chemistry, Korea University, Seoul 02841, Republic of Korea

Jeong Hyeon Jo − *Therapeutics and Biotechnology Division, Korea Research Institute of Chemical Technology (KRICT), Daejeon 34114, Republic of Korea; Graduate School of New Drug Discovery and Development, Chungnam National University, Daejeon 34134, Republic of Korea*

KyungJin Lee − *Department of Microbiology, CHA University School of Medicine, Seongnam 13488, Republic of Korea; ORGANOIDSCIENCES, Seongnam 13488, Republic of Korea*

Dong Hyuck Bae − *Department of Microbiology, CHA University School of Medicine, Seongnam 13488, Republic of Korea*

Tae-Young Kim − *School of Earth Sciences & Environmental Engineering, Gwangju Institute of Science and Technology (GIST), Gwangju 61005, Republic of Korea;* orcid.org/0000-0002-8846-3338

Complete contact information is available at: https://pubs.acs.org/10.1021/acsomega.4c05039

Author Contributions

◆B.K., Y.E.K., S.B.P., S.S.K., J.L., J.H.J., M.A.B., D.K., K.Y.K. contributed equally to this work. M.A.B., D.K., T.-Y.K., S.−H.C. and K.Y.K. conceived the project and was responsible for the overall experimental design. B.K., Y.E.K., S.B.P., S.S.K., J.H.J., and J.L. performed experiments and analyzed all data presented. B.K., Y.E.K., S.S.K., and J.L. wrote the manuscript with input from all authors.

Notes

The authors declare no competing financial interest.

■ ACKNOWLEDGMENTS

The authors greatly acknowledge financial support from the Ministry of Science and ICT (2021R1A2C2011195), the Ministry of Trade, Industry & Energy (20009774) and the Korea Research Institute of Chemical Technology (SI2231-40, KK2452-10, KK2431-10) of Republic of Korea.

■ REFERENCES

(1) Miller, I. O.; Sotero de Menezes, M. A. SCN1A Seizure Disorders. In *GeneReviews*; Adam, M. P.; Feldman, J.; Mirzaa, G. M.; Pagon, R. A.; Wallace, S. E.; Bean, L. J.; Gripp, K. W.; Amemiya, A., Eds.; University of Washington: Seattle: Seattle (WA), 1993.

(2) Bender, A. C.; Morse, R. P.; Scott, R. C.; Holmes, G. L.; Lenck-Santini, P.-P. SCN1A Mutations in Dravet Syndrome: Impact of Interneuron Dysfunction on Neural Networks and Cognitive Outcome. *Epilepsy Behav.* **2012**, *23* (3), 177−186.

(3) Valassina, N.; Brusco, S.; Salamone, A.; Serra, L.; Luoni, M.; Giannelli, S.; Bido, S.; Massimino, L.; Ungaro, F.; Mazzara, P. G.; D'Adamo, P.; Lignani, G.; Broccoli, V.; Colasante, G. Scn1a Gene Reactivation after Symptom Onset Rescues Pathological Phenotypes in a Mouse Model of Dravet Syndrome. *Nat. Commun.* **2022**, *13* (1), No. 161.

(4) Tahara, M.; Higurashi, N.; Hata, J.; Nishikawa, M.; Ito, K.; Hirose, S.; Kaneko, T.; Mshimo, T.; Sakuma, T.; Yamamoto, T.; Okano, H. J. Developmental changes in brain activity of heterozygous SCN1A knockout rats. *Front. Neurol.* **2023**, *14* (14), No. 1125089.

(5) Das, A.; Zhu, B.; Xie, Y.; Zeng, L.; Pham, A. T.; Neumann, J. C.; Safrina, O.; Benavides, D. R.; MacGregor, G. R.; Schutte, S. S.; Hunt, R. F.; O'Dowd, D. K. Interneuron Dysfunction in a New Mouse Model of SCN1A GEFS+. *eNeuro* **2021**, *8* (2), No. ENEURO.0394−20.2021, DOI: 10.1523/ENEURO.0394-20.2021.

(6) Lancaster, M. A.; Knoblich, J. A. Generation of Cerebral Organoids from Human Pluripotent Stem Cells. *Nat. Protoc.* **2014**, *9* (10), 2329−2340.

(7) Sloan, S. A.; Andersen, J.; Paşca, A. M.; Birey, F.; Paşca, S. P. Generation and Assembly of Human Brain Region-Specific Three-Dimensional Cultures. *Nat. Protoc.* **2018**, *13* (9), 2062−2085.

(8) Cakir, B.; Xiang, Y.; Tanaka, Y.; Kural, M. H.; Parent, M.; Kang, Y.-J.; Chapeton, K.; Patterson, B.; Yuan, Y.; He, C.-S.; Raredon, M. S. B.; Dengelegi, J.; Kim, K.-Y.; Sun, P.; Zhong, M.; Lee, S.; Patra, P.; Hyder, F.; Niklason, L. E.; Lee, S.-H.; Yoon, Y.-S.; Park, I.-H. Engineering of Human Brain Organoids with a Functional Vascular-like System. *Nat. Methods* **2019**, *16* (11), 1169−1175.

(9) Eichmüller, O. L.; Knoblich, J. A. Human Cerebral Organoids - a New Tool for Clinical Neurology Research. *Nat. Rev. Neurol.* **2022**, *18* (11), 661−680.

(10) Tsugawa, H.; Cajka, T.; Kind, T.; Ma, Y.; Higgins, B.; Ikeda, K.; Kanazawa, M.; VanderGheynst, J.; Fiehn, O.; Arita, M. MS-DIAL: Data-Independent MS/MS Deconvolution for Comprehensive Metabolome Analysis. *Nat. Methods* **2015**, *12* (6), 523−526.

(11) Adlakha, Y. K. Human 3D Brain Organoids: Steering the Demolecularization of Brain and Neurological Diseases. *Cell Death Discovery* **2023**, *9* (1), No. 221.

(12) Steinberg, D. J.; Repudi, S.; Saleem, A.; Kustanovich, I.; Viukov, S.; Abudiab, B.; Banne, E.; Mahajnah, M.; Hanna, J. H.; Stern, S.; Carlen, P. L.; Aqeilan, R. I. Modeling Genetic Epileptic Encephalopathies Using Brain Organoids. *EMBO Mol. Med.* **2021**, *13* (8), No. e13610.

(13) Nieto-Estévez, V.; Hsieh, J. Human Brain Organoid Models of Developmental Epilepsies. *Epilepsy Curr.* **2020**, *20* (5), 282−290.

(14) Baldassari, S.; Musante, I.; Iacomino, M.; Zara, F.; Salpietro, V.; Scudieri, P. Brain Organoids as Model Systems for Genetic Neurodevelopmental Disorders. *Front. Cell Dev. Biol.* **2020**, *8*, No. 590119, DOI: 10.3389/fcell.2020.590119.

(15) Salick, M. R.; Lubeck, E.; Riesselman, A.; Kaykas, A. The Future of Cerebral Organoids in Drug Discovery. *Semin. Cell Dev. Biol.* **2021**, *111*, 67−73.

(16) Feldberg, W. The Role of Acetylcholine in the Central Nervous System. *Br. Med. Bull.* **1950**, *6* (4), 312−321.

(17) Roberts, E.; Frankel, S. Gamma-Aminobutyric Acid in Brain: Its Formation from Glutamic Acid. *J. Biol. Chem.* **1950**, *187* (1), 55−63.

(18) Vianna, M. R.; Izquierdo, L. A.; Barros, D. M.; Walz, R.; Medina, J. H.; Izquierdo, I. Short- and Long-Term Memory: Differential Involvement of Neurotransmitter Systems and Signal Transduction Cascades. *An Acad. Bras. Cienc.* **2000**, *72* (3), 353−364.

(19) Shiah, I. S.; Yatham, L. N. GABA Function in Mood Disorders: An Update and Critical Review. *Life Sci.* **1998**, *63* (15), 1289−1303.

(20) Park, S. B.; Koh, B.; Kwon, H. S.; Kim, Y. E.; Kim, S. S.; Cho, S.-H.; Kim, T.-Y.; Bae, M. A.; Kang, D.; Kim, C. H.; Kim, K. Y. Quantitative and Qualitative Analysis of Neurotransmitter and Neurosteroid Production in Cerebral Organoids during Differentiation. *ACS Chem. Neurosci.* **2023**, *14* (20), 3761−3771.

(21) Zhu, K.; Bendl, J.; Rahman, S.; Vicari, J. M.; Coleman, C.; Clarence, T.; Latouche, O.; Tsankova, N. M.; Li, A.; Brennand, K. J.; Lee, D.; Yuan, G.-C.; Fullard, J. F.; Roussos, P. Multi-Omic Profiling of the Developing Human Cerebral Cortex at the Single-Cell Level. *Sci. Adv.* **2023**, *9* (41), No. eadg3754.

(22) Zheng, H.; Feng, Y.; Tang, J.; Ma, S. Interfacing Brain Organoids with Precision Medicine and Machine Learning. *Cell Rep. Phys. Sci.* **2022**, *3* (7), No. 100974.

(23) Mohammad-Zadeh, L. F.; Moses, L.; Gwaltney-Brant, S. M. Serotonin: A Review. *J. Vet. Pharmacol. Ther.* **2008**, *31* (3), 187−199.

(24) Klein, M. O.; Battagello, D. S.; Cardoso, A. R.; Hauser, D. N.; Bittencourt, J. C.; Correa, R. G. Dopamine: Functions, Signaling, and Association with Neurological Diseases. *Cell Mol. Neurobiol.* **2019**, *39* (1), 31−59.

(25) Tohgi, H.; Abe, T.; Hashiguchi, K.; Saheki, M.; Takahashi, S. Remarkable Reduction in Acetylcholine Concentration in the Cerebrospinal Fluid from Patients with Alzheimer Type Dementia. *Neurosci. Lett.* **1994**, *177* (1−2), 139−142.

(26) Owens, M. J.; Nemeroff, C. B. Role of Serotonin in the Pathophysiology of Depression: Focus on the Serotonin Transporter. *Clin. Chem.* **1994**, *40* (2), 288−295.
(27) Kim, S. S.; Kan, H.; Hwang, K.-S.; Yang, J. Y.; Son, Y.; Shin, D.-S.; Lee, B. H.; Ahn, S. H.; Ahn, J. H.; Cho, S.-H.; Bae, M. A. Neurochemical Effects of 4-(2Chloro-4-Fluorobenzyl)-3-(2-Thienyl)-1,2,4-Oxadiazol-5(4H)-One in the Pentylenetetrazole (PTZ)-Induced Epileptic Seizure Zebrafish Model. *Int. J. Mol. Sci.* **2021**, *22* (3), 1285.
(28) Bagdy, G.; Kecskemeti, V.; Riba, P.; Jakus, R. Serotonin and Epilepsy. *J. Neurochem.* **2007**, *100* (4), 857−873.
(29) Liguz-Lecznar, M.; Lehner, M.; Kaliszewska, A.; Zakrzewska, R.; Sobolewska, A.; Kossut, M. Altered Glutamate/GABA Equilibrium in Aged Mice Cortex Influences Cortical Plasticity. *Brain Struct. Funct.* **2015**, *220* (3), 1681−1693.
(30) Yuan, Y.; O'Malley, H. A.; Smaldino, M. A.; Bouza, A. A.; Hull, J. M.; Isom, L. L. Delayed Maturation of GABAergic Signaling in the Scn1a and Scn1b Mouse Models of Dravet Syndrome. *Sci. Rep* **2019**, *9* (1), No. 6210.
(31) Yu, F. H.; Mantegazza, M.; Westenbroek, R. E.; Robbins, C. A.; Kalume, F.; Burton, K. A.; Spain, W. J.; McKnight, G. S.; Scheuer, T.; Catterall, W. A. Reduced Sodium Current in GABAergic Interneurons in a Mouse Model of Severe Myoclonic Epilepsy in Infancy. *Nat. Neurosci.* **2006**, *9* (9), 1142−1149.
(32) Horn, A.; Jaiswal, J. K. Structural and Signaling Role of Lipids in Plasma Membrane Repair. *Curr. Top. Membr.* **2019**, *84*, 67−98.
(33) Corraliza-Gomez, M.; Sanchez, D.; Ganfornina, M. D. Lipid-Binding Proteins in Brain Health and Disease. *Front. Neurol.* **2019**, *10*, No. 1152.
(34) Yang, D.; Wang, X.; Zhang, L.; Fang, Y.; Zheng, Q.; Liu, X.; Yu, W.; Chen, S.; Ying, J.; Hua, F. Lipid Metabolism and Storage in Neuroglia: Role in Brain Development and Neurodegenerative Diseases. *Cell Biosci.* **2022**, *12* (1), No. 106.
(35) Kao, Y.-C.; Ho, P.-C.; Tu, Y.-K.; Jou, I.-M.; Tsai, K.-J. Lipids and Alzheimer's Disease. *Int. J. Mol. Sci.* **2020**, *21* (4), 1505.
(36) Yadav, R. S.; Tiwari, N. K. Lipid Integration in Neurodegeneration: An Overview of Alzheimer's Disease. *Mol. Neurobiol.* **2014**, *50* (1), 168−176.
(37) Udagawa, J.; Hino, K. Plasmalogen in the Brain: Effects on Cognitive Functions and Behaviors Attributable to Its Properties. *Brain Res. Bull.* **2022**, *188*, 197−202.
(38) Dorninger, F.; Forss-Petter, S.; Berger, J. From Peroxisomal Disorders to Common Neurodegenerative Diseases - the Role of Ether Phospholipids in the Nervous System. *FEBS Lett.* **2017**, *591* (18), 2761−2788.
(39) Senanayake, V.; Goodenowe, D. B. Plasmalogen Deficiency and Neuropathology in Alzheimer's Disease: Causation or Coincidence? *Alzheimers Dement* **2019**, *5*, 524−532.
(40) Malheiro, A. R.; Correia, B.; Ferreira da Silva, T.; Bessa-Neto, D.; Van Veldhoven, P. P.; Brites, P. Leukodystrophy Caused by Plasmalogen Deficiency Rescued by Glyceryl 1-Myristyl Ether Treatment. *Brain Pathol.* **2019**, *29* (5), 622−639.
(41) Norman, E.; Cutler, R. G.; Flannery, R.; Wang, Y.; Mattson, M. P. Plasma Membrane Sphingomyelin Hydrolysis Increases Hippocampal Neuron Excitability by Sphingosine-1-Phosphate Mediated Mechanisms. *J. Neurochem.* **2010**, *114* (2), 430−439.
(42) Wang, Y.; Tan, B.; Wang, Y.; Chen, Z. Cholinergic Signaling, Neural Excitability, and Epilepsy. *Molecules* **2021**, *26* (8), 2258.
(43) Belelli, D.; Herd, M. B.; Mitchell, E. A.; Peden, D. R.; Vardy, A. W.; Gentet, L.; Lambert, J. J. Neuroactive Steroids and Inhibitory Neurotransmission: Mechanisms of Action and Physiological Relevance. *Neuroscience* **2006**, *138* (3), 821−829.
(44) Romo-Parra, H.; Blaesse, P.; Sosulina, L.; Pape, H.-C. Neurosteroids Increase Tonic GABAergic Inhibition in the Lateral Section of the Central Amygdala in Mice. *J. Neurophysiol.* **2015**, *113* (9), 3421−3431.
(45) Samba Reddy, D.; Ramanathan, G. Finasteride Inhibits the Disease-Modifying Activity of Progesterone in the Hippocampus Kindling Model of Epileptogenesis. *Epilepsy Behav.* **2012**, *25* (1), 92−97.
(46) Ghadiri, T.; Vakilzadeh, G.; Hajali, V.; Khodagholi, F. Progesterone Modulates Post-Traumatic Epileptogenesis through Regulation of BDNF-TrkB Signaling and Cell Survival-Related Pathways in the Rat Hippocampus. *Neurosci. Lett.* **2019**, *709*, No. 134384.
(47) de Kloet, E. R.; Karst, H.; Joëls, M. Corticosteroid Hormones in the Central Stress Response: Quick-and-Slow. *Front. Neuroendocrinol.* **2008**, *29* (2), 268−272.
(48) Zhang, J.; Liu, Q. Cholesterol Metabolism and Homeostasis in the Brain. *Protein Cell* **2015**, *6* (4), 254−264.
(49) Foley, R. A.; Sims, R. A.; Duggan, E. C.; Olmedo, J. K.; Ma, R.; Jonas, S. J. Delivering the CRISPR/Cas9 System for Engineering Gene Therapies: Recent Cargo and Delivery Approaches for Clinical Translation. *Front. Bioeng. Biotechnol.* **2022**, *10*, No. 973326.
(50) Lotfi, M.; Morshedi Rad, D.; Mashhadi, S. S.; Ashouri, A.; Mojarrad, M.; Mozaffari-Jovin, S.; Farrokhi, S.; Hashemi, M.; Lotfi, M.; Ebrahimi Warkiani, M.; Abbaszadegan, M. R. Recent Advances in CRISPR/Cas9 Delivery Approaches for Therapeutic Gene Editing of Stem Cells. *Stem Cell Rev. Rep.* **2023**, *19* (8), 2576−2596.
(51) Xiang, Y.; Tanaka, Y.; Patterson, B.; Kang, Y.-J.; Govindaiah, G.; Roselaar, N.; Cakir, B.; Kim, K.-Y.; Lombroso, A. P.; Hwang, S.-M.; Zhong, M.; Stanley, E. G.; Elefanty, A. G.; Naegele, J. R.; Lee, S.-H.; Weissman, S. M.; Park, I.-H. Fusion of Regionally Specified hPSC-Derived Organoids Models Human Brain Development and Interneuron Migration. *Cell Stem Cell* **2017**, *21* (3), 383−398.e7. 007.
(52) Kim, S. S.; Lee, H.-Y.; Song, J. S.; Bae, M.-A.; Ahn, S. UPLC-MS/MS-Based Profiling of 31 Neurochemicals in the Mouse Brain after Treatment with the Antidepressant Nefazodone. *Microchem. J.* **2021**, *169*, No. 106580.
(53) Lindeboom, R. G.; van Voorthuijsen, L.; Oost, K. C.; Rodríguez-Colman, M. J.; Luna-Velez, M. V.; Furlan, C.; Baraille, F.; Jansen, P. W.; Ribeiro, A.; Burgering, B. M.; Snippert, H. J.; Vermeulen, M. Integrative Multi-Omics Analysis of Intestinal Organoid Differentiation. *Mol. Syst. Biol.* **2018**, *14* (6), No. e8227.
(54) Cox, J.; Mann, M. MaxQuant Enables High Peptide Identification Rates, Individualized p.p.b.-Range Mass Accuracies and Proteome-Wide Protein Quantification. *Nat. Biotechnol.* **2008**, *26* (12), 1367−1372.
(55) Tyanova, S.; Temu, T.; Sinitcyn, P.; Carlson, A.; Hein, M. Y.; Geiger, T.; Mann, M.; Cox, J. The Perseus Computational Platform for Comprehensive Analysis of (Prote)Omics Data. *Nat. Methods* **2016**, *13* (9), 731−740.

https://doi.org/10.1021/acsomega.4c05039
ACS Omega 2024, 9, 39804−39816